A&A 530, A136 (2011)
DOI: 10.1051/0004-6361/201016369

Astronomy & Astrophysics

The flare model for X-ray variability of NGC 4258

T. Trześniewski[1], B. Czerny[2], V. Karas[3], T. Pecháček[3], M. Dovčiak[3], R. Goosmann[4], and M. Nikołajuk[5]

[1] Institute of Physics, Jagiellonian University, Reymonta 4, 30059 Krakow, Poland
[2] Copernicus Astronomical Center, Bartycka 18, 00716 Warsaw, Poland
[3] Astronomical Institute, Academy of Sciences, Boční II 1401, 14131 Prague, Czech Republic
e-mail: vladimir.karas@cuni.cz
[4] Observatoire Astronomique de Strasbourg, 67000 Strasbourg, France
[5] Faculty of Physics, University of Białystok, Lipowa 41, 15424 Białystok, Poland

Received 20 December 2010 / Accepted 18 April 2011

ABSTRACT

Aims. We study the variability mechanism of active galactic nuclei (AGN) within the framework of the flare model. We examine the case of Seyfert/LINER galaxy NGC 4258, which is observed at high inclination angle and exhibits rapid fluctuations in its X-ray light curve.

Methods. We construct a model light curve based on the assumption of magnetic flares localized in the equatorial plane and orbiting with Keplerian speed at each given radius. We calculate the level of variability as a function of the inclination of an observer, taking into account all effects of general relativity near a rotating supermassive black hole.

Results. The variability level is a monotonic function of the source inclination. It rises more rapidly for larger values of the black hole spin (Kerr parameter a) and for steeper emissivity (index β of the radial profile). We compare the expected level of variability for the viewing angle 81.6 deg, as inferred for NGC 4258, with the case of moderate viewing angles of about 30 deg, which are typical of Seyfert type-1 galaxies.

Conclusions. Highly inclined sources such as this one are particularly suitable to test the flare model because the orbital motion, Doppler boosting, and light bending are all expected to have maximum effect when the accretion disk is seen almost edge-on. The model is consistent with the NGC 4258 variability, where the obscuring material is thought to be localized mainly toward the equatorial plane rather than forming a geometrically thick torus. Once the intrinsic timescales of the flare duration are determined with higher precision, this kind of highly inclined objects with a precisely known mass of the black hole can be used to set independent constraints on the spin parameter.

Key words. accretion, accretion disks – galaxies: active – galaxies: Seyfert – X-rays: galaxies

1. Introduction

For many years the X-ray emission of active galactic nuclei (AGN) has been known to be strongly variable (see e.g. Gaskell et al. 2006; Uttley 2007, for reviews). However, the nature of this variability remains unknown. Most proposed models have been based on a natural assumption that the emission originates close to the accreting supermassive black hole and fluctuates on the dynamical timescale. Rapid variability is among the arguments in favor of this interpretation (Krolik 1999). The effects of general relativity are expected to play an important role in shaping the observed signal (Kato et al. 1998).

As the innermost part of accretion flow likely proceeds through some form of a disk, characterized by a (roughly) Keplerian profile of rotational velocity, the relativistic effects are expected to depend on the inclination angle of the observer with respect to the disk plane. These effects are only weakly seen in the stationary continuum models if the emission is due to Comptonization, but they are very profound in the observed shapes of spectral features such as the iron Kα line (e.g. Fabian et al. 1995). In addition, earlier studies predict that non-stationary continuum models can display relativistic effects also through the dependence of the level of variability on the inclination angle of an observer (Zhang & Bao 1991; Abramowicz et al. 1991; Karas 1998; Fukue 2003; Czerny et al. 2004). Therefore, the application of a specific model to both low and high inclination sources opens an additional possibility of model testing.

In the present paper, we apply the flare model developed originally for the case of Seyfert galaxy MCG–6-30-15, which is a source at a moderate inclination ($\theta_o \sim 30$ deg) with respect to the observer's line of sight (Fabian et al. 1995, 2002), to the NGC 4258 galaxy viewed from the almost edge-on direction. This active galaxy is unique in several aspects: well-resolved maser emission from the nucleus allows an accurate mass determination of the black hole; the source is Compton thin (despite the high inclination), which allows us to measure the X-ray variability; rotation studies also show that the inner accretion disk follows Keplerian orbital motion very accurately.

The paper is organized as follows. In Sect. 2, we summarize the general scenario of the flare model, introduce a convenient parameterization, and adapt this scheme to the case of NGC 4258. We discuss the main differences in the model set-up caused by our concentration in previous papers on low to moderate inclinations for the application to unobscured Seyfert 1 AGN, whereas now we wish to apply the model to a highly-inclined source. In Sect. 3, we present our showing in particular the inclination dependence of the variability variance. We consider the role of the avalanche prescription, where the flares are mutually

interconnected as they occur in families. Finally we summarize the results in Sect. 4 and present our conclusions.

2. Flare model for X-ray variability of NGC 4258

2.1. Description of the flare model

The idea of X-ray emission coming from multiple locations within/above accretion disks around a black hole is motivated by the important role of magnetic fields in the process of accretion. The original formulation of the flare model by Galeev et al. (1979) was followed by numerous papers (e.g. Di Matteo 1998; Nayakshin & Kazanas 2001; Merloni & Fabian 2001; Collin et al. 2003; Goosmann et al. 2007b). A common theme to these models is an underlying assumption of a standard-type accretion flow driving the magnetic field. A similar picture can also be developed in the absence of a cold disk since in that case multiple shocks are expected to form in the hot accretion flow (e.g. Boettcher & Liang 1999; Życki 2003). The attractiveness of the flare model is also supported by the close correlation between the radio and X-ray emission in radio quiet AGN, which is a phenomenon typical of active stellar coronae (Laor & Behar 2008).

In the present work, we generalize the model developed by Czerny et al. (2004) and Goosmann et al. (2006). We parameterize the distribution of the flares across the disk and the flare properties. We assume that the luminosity of a single flare following the initial onset decreases gradually with time. This differs from the previous paper where we adopted a rectangular profile for the flare light curve. The most important modification is the introduction of a coupling between the flares through the presence of avalanches, as discussed e.g. by Poutanen & Fabian (1999), Życki (2002), and by Pecháček et al. (2008). Thus, our model follows the general idea of the scheme based on the propagation of perturbations (Mineshige et al. 1994; Lyubarskii 1997; Kotov et al. 2001; Arévalo & Uttley 2006; Titarchuk & Shaposhnikov 2008).

Spontaneous flares originate at a certain outer radius, $R_{\rm spont}$. Its value can be rather distant from the center, as this seems to follow from the discussion of well-studied cases of major flares in AGN (e.g. Ponti et al. 2004; Goosmann et al. 2007a). On a more theoretical side, Uzdensky & Goodman (2008) described a specific scenario of a magnetized corona above a turbulent accretion disk. Magnetic loops rise above the disk, where they become sheared by differential rotation of the field line foot-points until reconnection occurs. These events are responsible for the occurrence of primary flares and the subsequent dissipation of magnetic energy.

Spontaneous flares are accompanied by avalanches of secondary flares developing subsequently inside $R_{\rm spont}$. The assumptions about the parent flare localization and the gradual avalanche progression towards smaller radii go beyond the standard avalanche model, which does not invoke any particular form of the spatial distribution. General arguments, based mainly on the diffusion equation for the propagation of the events, suggest that the properties of secondary flares are described by power-law distributions. In this way, the onset of variability occurs at large radii and induces secondary fluctuations further down the accretion flow, in the inner regions of the disk.

In our paper, the flares are assumed to vanish at the inner radius of the computational zone, $R_{\rm in}$, which corresponds to the final inflow of perturbations below the innermost stable circular orbit (ISCO), and eventually below the black hole horizon. The assumption about the exponential decay of individual flares is another improvement of our previous scheme (see Czerny et al. 2004, where we assumed a common characteristic lifetime for the duration of all flares which then switch off abruptly). Onset of flares followed by their rapid but gradual decay may be analogous to processes in solar flares, where similar mechanisms of heating via magnetic reconnection operate (e.g., Aschwanden et al. 1998).

2.2. Parameterization of the model

We briefly summarize the adopted parameterization. Flare events are characterized by radius from the black hole and the corresponding time of the occurrence. During their lifetime, the flares follow a coplanar Keplerian motion of the accretion disk.

As we wish to take general relativity effects into account, the flare event coordinates need to be defined in an appropriate manner. For the purposes of our investigation, the Boyer-Lindquist (t, r) coordinates suit well, because all flares are assumed to be distributed above the ISCO, so these coordinates are non-singular over the whole computational domain. An individual flare is located at the radius r and characterized by the moment of its birth, $t_{\rm birth}$. The flares rise instantaneously and decay with time t exponentially (with a sharp final cut-off)

$$f(t) = \begin{cases} f_1(r)\,\exp\left(-\epsilon\,\dfrac{t-t_{\rm birth}}{\tau(r)}\right), & t_{\rm birth} < t < t_{\rm birth}+\tau(r), \\ 0, & t > t_{\rm birth}+\tau(r) \text{ or } t<0. \end{cases} \quad (1)$$

The amplitude $f_1(r)$ of a flare depends on the flare location, and its dependence on the radial coordinate has the form

$$f_1(r) = f_0\,\left(\frac{r}{r_0}\right)^{-\beta}, \quad (2)$$

where f_0 is a normalization constant and β is a model parameter. The lifetime of the flare is assumed to be related to the flare location as

$$\tau(r) = \tau_0\,\left(\frac{r}{r_0}\right)^{\delta}, \quad (3)$$

where τ_0 and δ are the model parameters. The scaling radius r_0 was set at $18\,R_{\rm g}$.

In our picture, we assume that each flare can lead to a new flare with the probability given by a Poissonian distribution around a mean value μ. Each new flare is always generated closer to the black hole than the parent flare: the location of the new flare, $r_{\rm new}$, is derived from the radii between the parent flare radius, r, and the radius sr $(0 \le s < 1)$, where the radial distribution of the probability is defined as

$$p(r_{\rm new}|r) = n_0(r) r_{\rm new}^{\gamma+1}, \quad (4)$$

where n_0(r) is the local normalization constant depending on the position of the parent flare, and γ is a model parameter. The value $\gamma = 0$ describes the uniform distribution across the disk surface. The time of birth of a new flare is drawn uniformly from the time bin between the birth of the parent flare, t, and $f_{\rm delay}t$, where the dimensionless factor $f_{\rm delay}$ is of the order of a few units.

The level of variability is set by global parameters: the number of spontaneous flares, $N_{\rm f}$, and the total duration of the light curve, $T_{\rm tot}$. The size of the single emitting region is then identical for all flares. It is fixed by the number of flares present in the source and the average luminosity L of the source. Flares are in Keplerian motion around the black hole. All general relativity effects connected with light propagation toward an observer

are calculated using the KY code (for details see Dovčiak et al. 2004a,b). For that purpose, all emitting regions are assumed to be projected onto the equatorial plane.

The shape of the locally emitted spectrum is parameterized as a power law of a given slope, and the reflection component with arbitrary normalization is usually included in the model (Czerny et al. 2004; Goosmann et al. 2006).

2.3. Properties of NGC 4258

NGC 4258 (M 106) is a barred spiral galaxy with a low-luminosity, type 1.9 Seyfert nucleus, which is also classified as a LINER[1]. The nuclear source has a luminosity of $L \approx 10^{-4}\ L_{\rm Edd}$ (Fruscione et al. 2005) and $L_{2-10} = 3.31 \times 10^{40}$ erg/s in the 2−10 keV band. The geometrical distance to NGC 4258 can be inferred from the orbital motion of H_2O masers in its nucleus, as demonstrated for the first time by Herrnstein et al. (1999), obtaining (7.2 ± 0.3) Mpc. The mass measurement is reliable because the maser rotation curve is most accurately described by the Keplerian profile (Herrnstein et al. 2005). Since the radius of the inner masers, measured with the VLBI, corresponds to 2.8 mas, high-velocity masers yield a mass for the central black hole of $M = 3.78 \times 10^7\ M_\odot$ (Martin 2008). The corresponding Eddington luminosity is $L_{\rm Edd} = 47.5 \times 10^{44}\ \frac{\rm erg}{\rm s}$, hence $L \approx 0.00475 \times 10^{44}$ erg/s.

The masers indicate that the angle of inclination of the inner disk is high with respect to the observer line of sight: $\theta_{\rm o} \approx 81.6°$, where 90° represents edge-on orientation (Martin 2008). Wilkes et al. (1995) find that optical lines are strongly linearly polarized and that the position angle coincides with the plane of the maser disk. Intrinsically, the source is likely to be a Seyfert 2 galaxy because the emission lines seen in the polarized light have widths appropriate for this class of objects.

The source was classified in X-rays as an obscured low-luminosity active nucleus by the ASCA observation (Makishima 1994). It was observed at X-ray wavelengths by two high-spatial resolution instruments: Chandra (Young & Wilson 2004) and XMM-Newton (Pietsch & Read 2002). More recently, results derived from Suzaku observations have also been reported (Reynolds et al. 2009; Yamada et al. 2009). The nuclear emission is strongly variable (Markowitz & Uttley 2005; Reynolds et al. 2009; Yamada et al. 2009). It follows that the surrounding medium cannot be Compton-thick along the line of sight from the entire X-ray producing volume. The obscuration instead causes a partial absorption with the absorbing column $\sim 10^{23}$ cm^{-2} (Yang et al. 2007; Yamada et al. 2009). The obscuring material can be localized mainly towards the equatorial plane rather than form a geometrically thick torus.

The slope of the X-ray spectrum is typical of Seyfert galaxies, where the value $\Gamma \sim 1.7-2.0$ depends on the model details (Pietsch & Read 2002; Yang et al. 2007). The cold and narrow iron line comes from the outer region, whereas no broad line was required to fit the XMM-Newton spectrum of this source (Yang et al. 2007; Reynolds et al. 2009). Yamada et al. (2009) confirm a significant X-ray variability and conclude that a classical geometrically thick torus does not seem to be present in this object, but that instead, the obscuration may take place along the line of sight close to the equatorial plane (e.g., Bao & Stuchlík 1992; Karas & Bao 1992).

[1] See The NASA/IPAC Extragalactic Database (NED), which is operated by the Jet Propulsion Laboratory, California Institute of Technology, under contract with the National Aeronautics and Space Administration.

2.4. X-ray excess variance in NGC 4258 and the enhancement ratio

The X-ray flux of NGC 4258 is highly variable. The level of this variability is conveniently characterized by the dimensionless excess variance (Nandra et al. 1997a)

$$(\mathtt{rms/mean})^2 = \frac{1}{N\mu^2}\sum_{i=1}^{N}[(X_i-\mu)^2-\sigma_i^2], \tag{5}$$

where N is the number of (equally spaced in time) data points, X_i is the count rate in a given time bin, μ is an unweighted arithmetic mean of X_i, and σ_i is the measurement error (predominantly consisting of Poissonian noise). The error level depends on the duration of the light curve. This dependence is a typical property of the sources dominated by the red noise, as discussed for example by Vaughan et al. (2003).

The source was observed several times with the ASCA satellite. These data were used by Nikołajuk et al. (2009), who obtained

$$(\mathtt{rms/mean})^2_{\rm observed} = 6.215^{+1.566}_{-2.350} \times 10^{-3} \tag{6}$$

for several light curves of typical total duration $T = 31\,300$ s, consisting of 50 bins and the duration time of a single bin $t_{\rm b} = 626$ s.

Since the black hole mass in NGC 4258 is known, this value can be compared to the expected variance from the relation between the black hole mass and the X-ray excess variance, that is characteristic of Seyfert galaxies (Nikołajuk et al. 2006, 2009)

$$(\mathtt{rms/mean})^2 = C\frac{T-2t_{\rm b}}{M}, \tag{7}$$

where $C = 1.92\ M_\odot\ {\rm s}^{-1}$.

For the black hole mass $3.78 \times 10^7\ M_\odot$ (see Sect. 2.3) and the light curve parameters T and $t_{\rm b}$ as above, we obtain

$$(\mathtt{rms/mean})^2_{\rm expected} = 1.52 \times 10^{-3}. \tag{8}$$

We thus define the enhancement ratio

$$\mathcal{R} = \frac{(\mathtt{rms/mean})^2_{\rm observed}}{(\mathtt{rms/mean})^2_{\rm expected}}, \tag{9}$$

and in the case of our source this ratio is equal to

$$\mathcal{R} = 4 \pm 1. \tag{10}$$

This (rather large) error arises mainly from the systematic error in the constant C in Eq. (7).

We expect that the enhancement is due to the inclination of the source, which in the case of NGC 4258 is significantly larger than the average inclination (about 30 deg) of sources usually used to derive the Eq. (7) (see e.g. Nikołajuk et al. 2006).

2.5. Adaptation of the model to NGC 4258

In our calculations, we used values of the black hole mass and an AGN luminosity appropriate for NGC 4258 given in the previous subsection. For the physical structure of the model, because of the lack of hard evidence of a disk in the vicinity of a black hole in the NGC 4258 nucleus, we assumed that only primary emission, from the flares, is present (no cold accretion disk, therefore, no spots are induced by flares on the disk surface). We assume that this emission is concentrated all around the equatorial plane.

Some model parameters were constrained to obtain a profile of the X-ray power-spectral density that is close to that for MCG–6-15-30 as a general representation of the observed shape for AGN. The values of the model parameters that we did not vary are as follows: $\delta = 1.5$ (assuming that flare duration scales with local Keplerian timescale), $\gamma = 1.5$, $s = 0.2$, $f_{\rm delay} = 7$, $\mu = 1.1$, and $R_{\rm out} = 200$. Dimensionless distances are given in units of the black hole gravitational radius, $R_{\rm g} \equiv GM/c^2$. Our model of course allows us to change the above-mentioned parameters if the physical reasoning requires us to use different values. We tested the model dependence on the luminosity concentration given by β (see Eq. (2)), on the proportionality constant of the flare duration, τ_0 (see Eq. (3)), and on the Kerr parameter, a.

The quantities in physical units, namely, the mass, spin, and distances, are related to the corresponding values in geometrical units

$$\frac{M^{\rm phys}}{M_\odot^{\rm phys}} = \frac{M}{1.477\times10^5\ {\rm cm}}, \quad a^{\rm phys} = ca, \quad r^{\rm phys} = r. \tag{11}$$

Furthermore,

$$\frac{a}{M} = \frac{a^{\rm phys}}{GM^{\rm phys}/c}, \quad \frac{r}{M} = \frac{r^{\rm phys}}{GM^{\rm phys}/c^2}. \tag{12}$$

We employ geometrical units in numerical simulations, but convert them to physical units interpreting the results. To obtain frequency in physical units [Hz], the relation is $\omega^{\rm phys} = c\omega$. The geometrized frequencies scale as M^{-1}. Their numerical values must thus be multiplied by a factor

$$\frac{c}{2\pi M} = (3.231\times10^4)\left(\frac{M}{M_\odot}\right)^{-1}\ [{\rm Hz}]. \tag{13}$$

To calculate the light curves, we followed the ASCA setup, as the source was observed several times with this satellite. This helps us to determine the excess variance to a sufficiently high precision (Nikołajuk et al. 2009). Therefore, in our calculations we applied the total duration of the observation $T = 31\,300$ s with 50 bins and the duration time of a single bin $t_{\rm b} = 626$ s.

Since the X-ray spectrum of NGC 4258 does not show the reflection component, the reflection must be either weak or absent. Therefore, in the present study we simplify the model and neglect the reflection. In this case, the additional parameter related to the normalization of the reflected component is unnecessary. The results in this case even more remarkably do not depend on the assumed slope of the power law emission.

For all model light curves, we calculated the variance and then tested its dependence on the inclination angle, while varying the Kerr parameter of the black hole and the radial distribution of the flare luminosity, β. The latter determines whether the emissivity is more or less concentrated toward the black hole.

3. Results: dependence of variance on inclination

We use the aforementioned model to calculate the normalized X-ray excess variance, $(\texttt{rms/mean})^2$, paying special attention to the relation between this quantity and the observer inclination. The flare model variability is very sensitive to the inclination, so we first explore this dependence while several other model parameters are kept fixed. In particular, we set the black hole mass to the appropriate value for NGC 4258. As for the black hole rotation, since we have no constraints for the spin parameter in NGC 4258, we also keep it free and analyze the level of variability for different values of a.

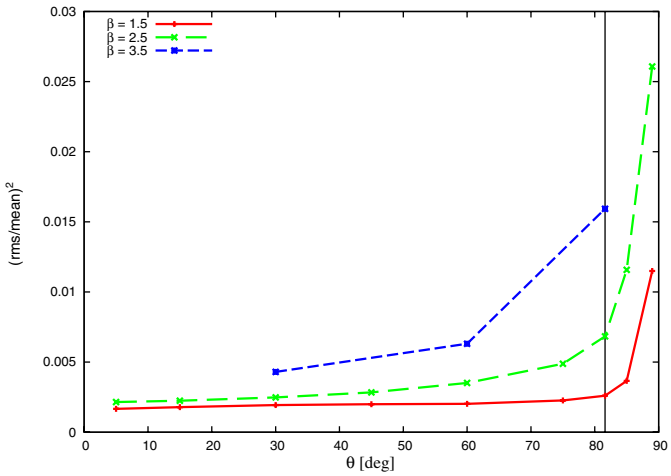

Fig. 1. The dependence of the normalized variance on the inclination angle of an observer for three emissivity profiles β for the Kerr black hole $a = 0.95$. The vertical line indicates the inclination of $\theta_{\rm o} = 81.6°$.

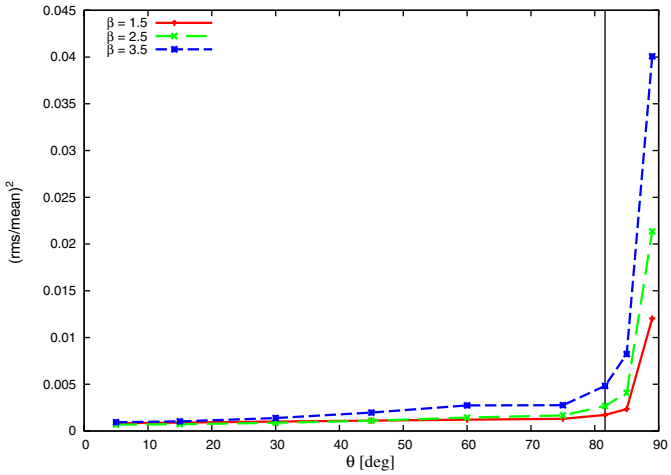

Fig. 2. The dependence of the normalized variance on the inclination angle for the same values of β as in the previous figure, but with a non-rotating (Schwarzschild, $a = 0$) black hole.

In Fig. 1, we plot the X-ray variance for three values of β assuming a rapidly rotating black hole (Kerr parameter $a = 0.95$). The value of $\beta \simeq 1.5$ corresponds to a shallow emissivity profile. The variability level increases with the inclination, first slowly and later sharply. The rise is the result of the beamed Doppler boosting at high inclinations, which is well-known from previous papers (e.g. Czerny et al. 2004; Dovčiak et al. 2008). The rise is faster for larger values of β, which implies that there is a larger contribution to the total luminosity of the source arising in the inner region. As a consequence, the relativistic effects are strongly enhanced.

The aforementioned increase in the variance with inclination is slower and the overall variability level is lower if the black hole is not rotating. In Fig. 2, we show the inclination dependence of the normalized variance for the same set of radial profiles β as in Fig. 1, but now with the Schwarzschild black hole. The ratio of the variances for $\beta = 3.5$ at $\theta_{\rm o} = 81.6°$ and $\theta_{\rm o} = 30°$ is equal to 3.5 for an $a = 0$ black hole, but increases to 3.7 for an $a = 0.95$ Kerr black hole in the presented plots.

The rise in the variance with the inclination angle is not a result of the statistical errors in simulations. It is well known that a single simulation of short timescale is strongly affected by the power leaking from the lower frequencies (Vaughan et al. 2003). However, in Figs. 1 and 2 the sequences for fixed values of β were calculated for the same realizations of the same statistical distribution. The rise in variance is entirely due to the change in the viewing angle. If we use different random realizations of the flare distribution the trend is less clear because of large statistical dispersion in the adopted length of the light curve. A single variance (in simulations as well as in the actual data) is determined with an accuracy of a factor of two.

Therefore, to show the model predictions to higher accuracy, we had to extend the simulated light curves by a factor of eight. For these longer light curves, we calculated the variance enhancement, defined as the ratio of the variance seen at 81.6° to that at 30°, as a function of the Kerr parameter. The result is shown in Fig. 3, for three values of the flare time-scale duration. We also plot the ratio of the observed variance, given in Eq. (6), to the variance expected from Eq. (4) of Nikołajuk et al. (2009). This ratio is found to equal 4.0, its standard deviation (1σ) error coming from the errors in both the variance and in scaling constant. Because of a lack of information about the black hole spin, the observational constraint is indicated by straight lines irrespective of the value of a.

The variance enhancement, in general, increases with the Kerr parameter but the detailed profile depends on the assumed scaling factor of the flare lifetime. The variability is yet greater when the flare lifetime close to the black hole is comparable to the time spent by the flare in the region of the highest Doppler boosting. The angular extension of this region (as a fraction of 2π) decreases as the Kerr parameter increases (Dovčiak et al. 2004a).

The enhanced variability is consistent with the expectations of the relativistic enhancement, within the framework of the flare model. A flare duration of longer timescale, $\tau_0 = 10^4$ s, is indicative of a non-rotating black hole, while the flares scaled down to $\tau_0 = 10^3$ s probably correspond to a spinning black hole with $a > 0.5$. However, taking into account the large error in the observed variance and the lack of a priori knowledge of the flare timescale we cannot at this stage make any firm conclusion about the black hole rotation in NGC 4258.

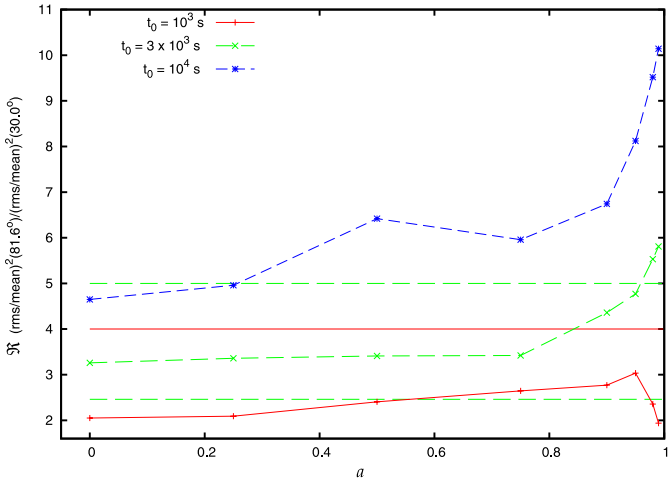

Fig. 3. The ratio $\mathcal{R}$ of normalized variance at the observer inclination angle $\theta_o = 81.6°$ with respect to the case $\theta_o = 30°$. The dependence on the dimensionless Kerr black hole parameter a is plotted for the assumed emissivity profile $\beta = 3.5$, for three values of the flare lifetime scale t_0, as indicated in the plot. Three horizontal lines give the enhancement ratio $\mathcal{R}$ for NGC 4258 given in Eq. (10) (middle line), and the range of errors (upper and lower lines). The simulated light curves were longer by factor 8 compared to those used in Figs. 1, 2.

4. Discussion

In the flare model of AGN X-ray variability the change in the X-ray flux is caused by a combination of two main effects. The first is the intrinsic variability of both a single flare and the flare distribution. The second is the variation caused by the relativistic effects of the flare orbital (Keplerian) motion. Analyzing the change in the level of variability with the inclination we can disentangle those two effects.

We chose NGC 4258 as a target of our study because of its exceptional properties. The source is highly inclined, seen almost edge-on, but is nevertheless Compton thin and the variable primary emission is still transmitted effectively through the material located at the source equatorial plane, although the X-ray emission is significantly absorbed. In addition, the mass of the central black hole in this object is measured accurately thanks to the spatially resolved water maser emission.

On the other hand, we modified our original flare model (Czerny et al. 2004) by including the exponential decay of individual flares and the effect of an avalanche-type development of flares. On the other hand, we neglected the cold disk reflection. In NGC 4258, any manifestations of reflection features, such as the broad relativistic iron line and temporary spots on the disk surface, are strongly suppressed. We thus understand the situation by presuming that the central corona is the source of enhanced variability and the place where flares originate.

After developing a refined version of the model, we analyzed the dependence of the X-ray variance on the inclination angle. We noticed that the rise in the variability with the inclination angle is faster if the emissivity is more concentrated towards the black hole, which is the case for larger values of the β parameter. We compared the expected level of variability for the viewing angle 81.6 deg, as inferred for NGC 4258, with the case of moderate viewing angles $\theta_o \approx 30$ deg, which are typical of Seyfert 1 galaxies (Nandra et al. 1997b, 2007). Our model predicts that the variability increase is monotonic with inclination.

The observed variability level in NGC 4258 is indeed higher by a factor consistent with the measured value of the central black hole mass, which was determined with high accuracy in this source from water maser emission. The measured X-ray excess in this source is equal to $\sigma^2 = 6.215^{+1.566}_{-2.350} \times 10^{-3}$ (Nikołajuk et al. 2009). The expected variance from the Eq. (4) of Nikołajuk et al. (2009) is a factor of four lower (the aforementioned formula is satisfactory for typical low-inclination Seyfert galaxies). This means that the flare model of variability would be consistent with this object provided that the X-ray variance for a highly inclined source is a factor of four higher than it is for low-inclination sources for which the relation was scaled.

Several parameters determine the outcoming light curve in our model. The interplay between the parameters is in general quite complex because the signal depends on the initial distribution of parent flares, their subsequent propagation across the accretion disk towards the inner edge, as well as the avalanche mechanism generating the secondary flares. To capture this entire process, we introduced the flare rise time $t_{\rm birth}$ in Eq. (1), the index of radial distribution of flare amplitudes β in Eq. (2), the radial profile of flare lifetime δ in Eq. (3), and the index of radial probability distribution γ in Eq. (4). Furthermore, the secondary flare generation is described by the parameters s, $f_{\rm delay}$,

μ, $R_{\rm in}$, and $R_{\rm out}$, which define the development and the gradual decay of the avalanches.

Despite the complicated picture given by the number of free parameters described above, it is interesting to note that only in special (but quite representative) cases do some parameters play an important role. This is in particular the case of a stationary distribution that is expected to arise when the secondary flares occur over the whole range of radii in the accretion disk ($s \to 0$). One can then check that the stationary situation depends sensitively on μ (i.e., the mean value of secondary flares) but the degree of the dependence on other parameters is much weaker.

5. Conclusions

The above-mentioned rise of variability agrees with the model prediction for a steep emissivity profile and the flare normalization timescale of 10^3–10^4 s. Higher values of the flare timescales are consistent with the low values of the black hole spin in NGC 4258, whereas shorter timescales are consistent with a rapidly spinning black hole.

The observed enhancement in variability supports the view that the X-ray emission is generated close to the black hole and subject to strong general relativity effects. This does not imply that the emission originates preferentially from magnetic flares above the disk, or that it instead comes from individual shocks in an optically thin inner flow that undergoes Keplerian motion. In the absence of a reflection component, our model is unable to differentiate between the two aforementioned scenarios. However, if the inflow is almost spherical, as in the models of Shrader & Titarchuk (1998) and Ishibashi & Courvoisier (2009), the variability enhancement is not expected for high inclination sources. The observed enhancement of variability of NGC 4258 thus implies that there is a significant azimuthal motion in the X-ray emitting plasma of the inner accretion disk.

Once the intrinsic timescales of the flare duration are determined with higher precision, the highly inclined objects with precisely known black hole masses can be used to set independent constraints on the spin parameter. The highly inclined AGNs that are not Compton thick and at the same time exhibit maser sources, such as NGC 4258, do exist (even though they are rather rare) and should be ideal candidates to apply the method described in this paper. We will however need to obtain a better coverage of their variability properties. It appears that unabsorbed Seyfert 2 galaxies (Brightman & Nandra 2008) or even dust-poor quasars (Hao et al. 2010) form a category of sources that could be suitable candidates.

Acknowledgements. This work was supported by grants 1P03D00829 and NN 203 380136 of the Polish Ministry of Science and Education, and the grant ME09036 of the Czech Ministry of Education, Youth and Sports. The work was carried out partially within the framework of the European Associated Laboratory "Astrophysics Poland–France" and the COST Action MP0905 "Black Holes in a Violent Universe". V.K. and M.D. acknowledge the Czech Science Foundation grants 205/07/0052 and 202/09/0772; T.P. acknowledges a postdoctoral grant No. 205/09/P468.

References

Abramowicz, M. A., Bao, G., Lanza, A., & Zhang, X.-H. 1991, A&A, 245, 454
Arévalo, P., & Uttley, P. 2006, MNRAS, 367, 801
Aschwanden, J., Dennis, B. R., & Benz, A. O. 1998, ApJ, 497, 972
Bao, G., & Stuchlík, Z. 1992, ApJ, 400, 163
Boettcher, M., & Liang, E. P. 1999, ApJ, 511, L37
Brightman, M., & Nandra, K. 2008, MNRAS, 390, 1241
Di Matteo, T. 1998, MNRAS, 299, L15
Collin, S., Coupe, S., Dumont, A.-M., Petrucci, P.-O., & Różańska, A. 2003, A&A, 400, 437
Czerny B., Różańska A., Dovčiak M., Karas V., & Dumont A.-M. 2004, A&A, 420, 1
Dovčiak, M., Karas, V., & Yaqoob, T. 2004a, ApJS, 153, 205
Dovčiak, M., Karas, V., Martocchia, A., Matt, G., & Yaqoob, T. 2004b, in Black Holes and Neutron Stars, Proc. of RAGtime 4/5 Workshops, ed. S. Hledík, & Z. Stuchlík, Silesian Univ., Opava, 33
Dovčiak, M., Karas, V., Matt, G., & Goosmann, R. W. 2008, MNRAS, 384, 361
Fabian, A. C., Nandra, K., Reynolds, C. S., et al. 1995, MNRAS, 277, L11
Fabian, A. C., Vaughan, S., Nandra, K., et al. 2002, MNRAS, 335, L1
Fruscione, A., Greenhill, L. J., Filippenko, A. V., et al. 2005, ApJ, 624, 103
Fukue J. 2003, PASJ, 55, 1121
Galeev, A. A., Rosner, R., & Vaiana, G. S. 1979, ApJ, 229, 318
Gaskell, C. M., McHardy, I. M., Peterson, B. M., & Sergeev, S. G. 2006, AGN Variability from X-rays to Radio Waves (San Francisco: ASP), ASP Conf. Ser., 360
Goosmann, R. W., Czerny, B., Mouchet, M., et al. 2006, A&A, 454, 741
Goosmann, R. W., Czerny, B., Karas, V., & Ponti, G. 2007a, A&A, 466, 865
Goosmann, R. W., Mouchet, M., Czerny, B., et al. 2007b, A&A, 475, 155
Hao, H., Elvis, M., Civano, F., et al. 2010, ApJ, 724, L59
Herrnstein, J. R., Moran, J. M., Greenhill, L. J., et al. 1999, Nature, 400, 539
Herrnstein, J. R., Moran, J. M., Greenhill, L. J., & Trotter, A. S. 2005, ApJ, 629, 719
Ishibashi, W., & Courvoisier, T. J.-L. 2009, A&A, 495, 113
Karas, V. 1998, MNRAS, 288, 12
Karas, V., & Bao, G. 1992, A&A, 257, 531
Kato, S., Fukue, J., & Mineshige, S. 1998, Black-Hole Accretion Disks (Kyoto: Kyoto University Press)
Kotov, O., Churazov, E., & Gilfanov, M. 2001, MNRAS, 327, 799
Krolik, J. H. 1999, Active Galactic Nuclei (Princeton: Princeton University Press)
Laor, A., & Behar, E. 2008, MNRAS, 390, 847
Lyubarskii, Yu. E. 1997, MNRAS, 292, 679
Makishima, K., Fujimoto, R., Ishisaki, Y., Kii, T., & Loewenstein, M. 1994, PASJ, 46, L77
Markowitz, A., & Uttley, P. 2005, ApJ, 625, L39
Martin, R. G. 2008, MNRAS, 624, 103
Merloni, A., & Fabian, A. C. 2001, MNRAS, 328, 958
Mineshige, S., Ouchi, N. B., & Nishimori, H. 1994, PASJ, 46, 97
Nandra, K., George, I. M., Mushotzky, R. F., Turner, T. J., & Yaqoob, T. 1997a, ApJ, 476, 70
Nandra, K., George, I. M., Mushotzky, R. F., Turner, T. J., & Yaqoob, T. 1997b, ApJ, 477, 602
Nandra, K., O'Neill, P. M., George, I. M., & Reeves, J. N. 2007, MNRAS, 382, 19
Nayakshin, S., & Kazanas, D. 2001, ApJ, 553, L141
Nikołajuk, M., Czerny, B., Ziółkowski, J., & Gierliński, M. 2006, MNRAS, 370, 1534
Nikołajuk, M., Czerny, B., & Gurynowicz, P. 2009, MNRAS, 394, 2141
Pecháček, T., Karas, V., & Czerny, B. 2008, A&A, 487, 815
Pietsch, W., & Read, A. M. 2002, A&A, 384, 793
Ponti, G., Cappi, M., Dadina, M., & Malaguti, G. 2004, A&A, 417, 451
Poutanen, J., & Fabian, A. C. 1999, MNRAS, 306, L31
Reynolds, C. S., Nowak, M. A., Markoff, S., et al. 2009, ApJ, 691, 1159
Shrader, C., & Titarchuk, L. 1998, ApJ, 499, L31
Titarchuk, L., & Shaposhnikov, N. 2008, ApJ, 678, 1230
Uttley, P. 2007, in The Central Engine of Active Galactic Nuclei, ASP Conf. Ser. 373, ed. L. C. Ho, & Jian-Min Wang, Xi'an, Xi'an Jioatong University, 149
Uzdensky, D. A., & Goodman, J. 2008, ApJ, 682, 608
Vaughan, S., Edelson, R., Warwick, R. S., & Uttley, P. 2003, MNRAS, 345, 1271
Wilkes, B. J., Schmidt, G. D., Smith, P. S., Mathur, S., & McLeod, K. K. 1995, ApJ, 455, L13
Yamada, S., Itoh, T., Makishima, K., & Nakazawa, K. 2009, PASJ, 61, 309
Yang, Y., Li, B., Wilson, A. S., & Reynolds, C. S. 2007, ApJ, 660, 1106
Young, A. J., & Wilson, A. S. 2004, ApJ, 601, 133
Zhang, X.-H., & Bao, G. 1991, A&A, 246, 21
Życki, P. T. 2002, MNRAS, 333, 800
Życki, P. T. 2003, MNRAS, 340, 639